JACS
JOURNAL OF THE AMERICAN CHEMICAL SOCIETY
Article
pubs.acs.org/JACS

Gold Nanorod@Chiral Mesoporous Silica Core–shell Nanoparticles with Unique Optical Properties

Wenjing Liu,[†,§] Zhening Zhu,[†,§] Ke Deng,[†] Zhengtao Li,[†] Yunlong Zhou,[†] Huibin Qiu,[‡] Yan Gao,*[,†] Shunai Che,*[,‡] and Zhiyong Tang*[,†]

[†]Laboratory of Nanomaterials, National Center for Nanoscience and Technology, Beijing 100190, People's Republic of China
[‡]School of Chemistry and Chemical Technology, State Key Laboratory of Composite Materials, Shanghai Jiao Tong University, 800 Dongchuan Road, Shanghai 200240, People's Republic of China

Supporting Information

ABSTRACT: The design and fabrication of chiral nanostructures is a promising approach to realize enantiomeric recognition and separation. In our work, gold nanorod@chiral mesoporous silica core–shell nanoparticles (GNR@CMS NPs) have been successfully synthesized. This novel material exhibits strong and tunable circular dichroism signals in the visible and near-infrared regions due to the optical coupling between the CMS shells and the GNR cores. When chiral cysteine molecules are loaded in the porous shells, the corresponding surface enhanced Raman scattering spectroscopy demonstrates a distinct chiral recognition effect, which can be used to semiquantitatively measure the composition of chiral enantiomers. A detailed sensing mechanism has been disclosed by density functional theory calculations.

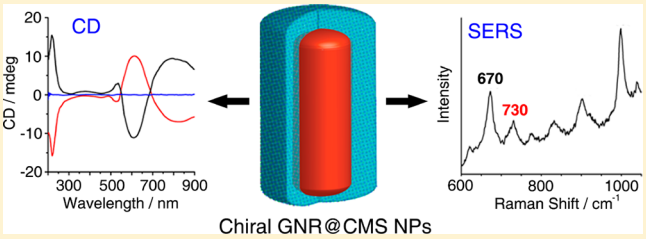

INTRODUCTION

Thanks to strong localized surface plasmon resonance (LSPR) characteristics, gold nanorods (GNRs) exhibit unique, aspect ratio dependent optical properties, which have attracted tremendous scientific interest and shown the potentials for a wide variety of applications.[1−5] With the fast development of synthesis techniques, GNRs with controllable geometries can be successfully prepared in large quantity and their optical properties are well tuned in the visible and near-infrared (near-IR) regions.[6−10] However, the poor stability of as-prepared GNRs (aggregation in solution or shape/size change under harsh conditions) restricts their practical applications in many fields such as optics, sensing, and catalysis.[11] Therefore, ligand exchange or additional coating on the GNR surface is necessary to preserve the structures and improve the properties for the desirable functionality.[12,13] Among the different methods, coating with a silica shell is becoming more attractive.[14−17] The employment of a silica coating not only provides high stability and chemical inertness but also allows subsequent functionalization and biocompatibility by chemically tailoring the surface of silica shells. Recently, porous silica shells, which have tunable and accessible pores and high surface area, have been coated on the surface of the GNRs for some important chemical and biological applications, such as catalytic reactions and drug delivery.[18−20] Nevertheless, current studies on the porous silica shells are focused on the utilization of their geometrical nature, e.g., containers for drugs and penetrating routes to the gold surface, and seldom attention has been paid to their functionalization for optical applications. As an example, the GNRs have been believed to be excellent substrates for highly sensitive surface enhanced Raman scattering (SERS) detection, since they are able to offer a much greater enhancement of the electromagnetic field in comparison with the spherical Au nanocrystals.[21,22] Unfortunately, though SERS measurements based on the GNRs have been utilized for detection of many molecules,[23−25] none of them have targeted chiral recognition due to the lack of optimal surface functionality of the GNRs.

Herein, we demonstrate successful coating of chiral mesoporous silica (CMS) shells on the surface of the GNRs by using amino acid derived chiral surfactants as the template molecules for shell growth.[26−29] Interestingly, the obtained gold nanorod@chiral mesoporous silica core–shell nanoparticles (GNR@CMS NPs) exhibit strong circular dichroism (CD) signals in the visible light and near-IR regions due to optical coupling between the GNRs and the chiral surfactants in the CMS shells. The CD activity can be fine-tuned through changing the aspect ratio of the GNRs. Furthermore, when cysteine (Cys) molecules of the same configuration with the shell-template molecules are loaded in the porous shells, a new band at 730 cm^{-1} appears in the SERS spectrum. Density functional theory (DFT) calculations reveal that the appearance of a peak at 730 cm^{-1} arises from the conformation change of chiral Cys molecules docked inside the CMS shells. More impressively, the ratio of the Cys enantiomers can be linearly measured by the intensity of the SERS peak at 730 cm^{-1}. This novel type of core–shell NPs in combination of the optical

Received: December 21, 2012
Published: June 6, 2013

   dx.doi.org/10.1021/ja312327m | J. Am. Chem. Soc. 2013, 135, 9659−9664

plasmonics from the GNR cores and the structural chirality from the CMS shells hold great promise for various applications in chiral sensors, enantioselective separation, and optical metamaterials.[30−36]

EXPERIMENTAL SECTION

Synthesis of GNRs. The GNRs were synthesized by a two-step seed-mediated growth method.[6] First, a seed solution was prepared in an aqueous solution of 0.075 M cetyltrimethylammonium bromide (CTAB) by reduction of 10 mL of 0.25 mM $HAuCl_4$ with 0.6 mM sodium borohydride as a reducing agent. Second, 12 μL of seed solution was added to a growth solution containing 0.1 M CTAB, 0.5 mM $HAuCl_4$, 0.55 mM ascorbic acid, and 0.06 mM silver nitrate. After 12 h, the solution of GNRs was centrifuged to remove the excess CTAB and redispersed in Milli-Q water.

Synthesis of Chiral Surfactants. Anionic surfactants derived from amino acids, including *N*-palmitoyl-L-phenylalanine (C_{16}-L-Phe), *N*-palmitoyl-D-phenylalanine (C_{16}-D-Phe), and *N*-palmitoyl-DL-phenylalanine (C_{16}-DL-Phe), were synthesized according to a previous report.[37] In a typical synthesis procedure of C_{16}-L-Phe, 0.1 mol of phenylalanine was dissolved in a mixture of water, acetone, and 0.1 mol of NaOH. Then 0.11 mol of palmitoyl chloride was added dropwise to this mixture under ice-cold conditions, while 10 M NaOH was used to maintain the pH value of the solution at 12. Subsequently, the mixture was stirred for an additional 1 h and acidified to pH 1 with HCl. The mixture was then washed thoroughly to neutralize the solution and remove the unreacted amino acid with deionized water. The precipitate was further washed with petroleum ether to remove the unreacted palmitoyl chloride. The final product was obtained by evaporating to dryness under vacuum.

Synthesis of GNR@CMS NPs. Our approach was performed by using chiral anionic surfactants as the templates and *N*-((trimethoxysilyl)propyl)-*N*,*N*,*N*-trimethylammonium chloride (TMAPS) as the costructure-directing agent. In a typical synthesis, C_{16}-L-Phe (0.101 g, 0.25 mmol) and aqueous NaOH solution (100 mM, 3 mL) were dissolved in a 20 mL solution of the as-purified GNR with stirring at room temperature. After the compounds were dissolved, 0.032 g of TMAPS and 0.070 g of tetraethylorthosilicate (TEOS) were added to the solution. The reaction was processed for 3 days, and the final products were centrifuged and redispersed in deionized water. The chiral templates were removed by mild extraction with HCl/ethanol 1/10 (v/v) solution under reflux for 12 h.

Loading Cys into the GNR@CMS NPs. A 1.5 mL portion of a freshly synthesized GNR@CMS NP solution was centrifuged and redispersed into 450 μL of deionized water. Subsequently, the solution was mixed with 50 μL of 4 mM Cys solution. Cys enantiomers of different ratios were prepared for the experiment.

Materials and Characterization. Tetrachloroauric acid, CTAB, and NaOH were purchased from Sinopharm. Silver nitrate, sodium borohydride, ascorbic acid, phenylalanine, and D-, L-, and DL-Cys were purchased from Alfa Aesar. TEOS, palmitoyl chloride, and TMAPS were purchased from TCI. All of the chemicals were used as received without further purification.

Scanning electron microscopy (SEM) measurements were performed on a Hitachi S4800 SEM at 10.0 kV. Characterizations of transmission electron microscopy (TEM) and high-angle annular dark-field scanning TEM energy dispersive X-ray spectroscopy (HAADF-STEM-EDS) mapping were carried out on a Tecnai G2 F20 U-TWIN instrument under an accelerating voltage of 200 kV. UV−vis and CD spectra were collected on a Hitachi U-3010 spectrophotometer and Jasco J-810 spectropolarimeter (using a quartz cuvette of 10 mm optical length), respectively. The nitrogen adsorption−desorption isotherms were measured on a Tristar3020 analyzer. SERS characterization was carried out by a confocal Raman spectroscope system (Renishaw inVia) with a HeNe laser (633 nm) as the light source for excitation. Powder XRD patterns were recorded on a D/MAX-TTRIII (CBO) instrument with Cu Kα radiation (λ =1.542 Å) operating at 50 kV and 300 mA.

Theoretical Calculations. The density functional theory (DFT) method was conducted to study the interaction energy between L-Cys and GNR@CMS templated by C_{16}-L-Phe and C_{16}-D-Phe. The interactions of Cys molecules with both the GNR surfaces and the mesoporous shells were considered. Details can be found in page S18 in the Supporting Information.

RESULTS AND DISCUSSION

Structural Characterization of GNR@CMS NPs. The morphologies of the GNR@CMS NPs were observed by both SEM and TEM (Figure 1). Figure 1a−c represents typical SEM

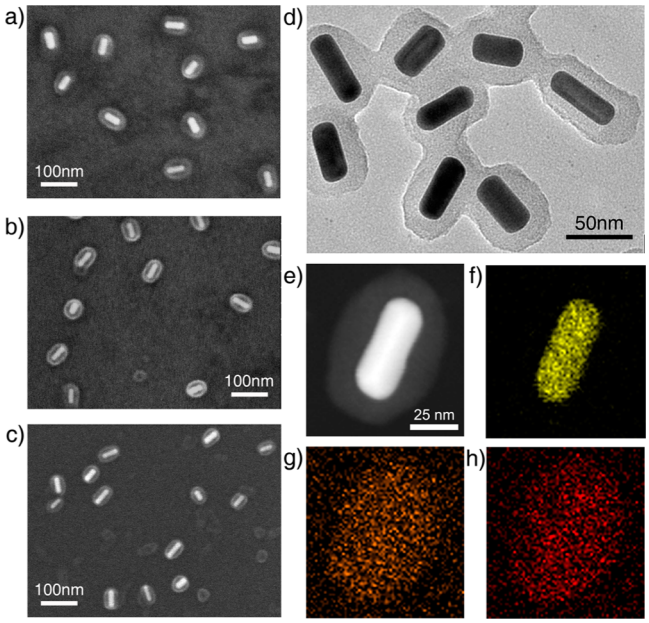

Figure 1. SEM images of the GNR@CMS NPs synthesized with three different chiral surfactants: (a) C_{16}-L-Phe; (b) C_{16}-D-Phe; (c) C_{16}-DL-Phe. (d) TEM image of GNR@CMS NPs. (e) HAADF-STEM image. HAADF-STEM-EDS mapping images of core−shell NPs: (f) Au mapping; (g) Si mapping; (h) O mapping.

images of the core−shell NPs with CMS shells templated by C_{16}-L-Phe, C_{16}-D-Phe, and C_{16}-DL-Phe, respectively. All three types of GNR@CMS NPs have identical sizes with diameters of ~45 nm and lengths of ~70 nm, and the silica shells on the GNRs are uniform with a thickness of ~15 nm (Figures S1−S3, Supporting Information). TEM (Figure 1d) and the corresponding HAADF-STEM-EDS (Figure 1e−h) were used to investigate the structures of the GNR@CMS NPs. The elemental mapping results clearly reveal that the NPs are composed of GNR cores and uniform silica shells (Figure 1e−h).

The crystal structures of GNR@CMS NPs were explored by XRD techniques (Figure 2). In the wide-angle XRD pattern (Figure 2a), four Au diffraction peaks are discerned at 2θ = 38.20, 44.42, 64.59, and 77.57°, which are assigned to (111), (200), (220), and (311) reflections of the face-centered cubic gold lattice, respectively. Furthermore, the small-angle XRD (SAXRD) measurement exhibits a clear and rather broad peak at 1.5−2°, corresponding to the characteristic peak of the ordered chiral mesoporous silica (Figure S4, Supporting Information).[27] The TEM image demonstrates that, after extraction, the mesoporous structure of the silica shells can be clearly discerned (Figure S5, Supporting Information). The nitrogen adsorption−desorption isotherm of the core−shell

dx.doi.org/10.1021/ja312327m | J. Am. Chem. Soc. 2013, 135, 9659−9664

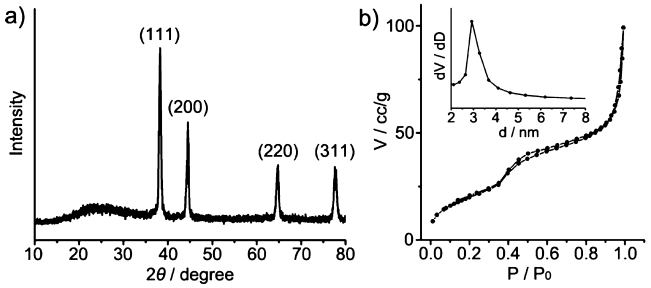

Figure 2. (a) Wide-angle XRD pattern and (b) N_2 adsorption–desorption isotherms of the extracted GNR@CMS NPs (inset in b: pore size distribution).

NPs after extraction exhibits an IV-type curve (Figure 2b). The pore size distribution made on the basis of the nitrogen adsorption isotherm represents a peak centered at the mean value of 2.9 nm (inset in Figure 2b). We also notice from Figure 2b that the BET (Brunauer–Emmett–Teller) specific surface area of core–shell NPs is around 75 m^2/g, which is considerably lower than that of pure CMS. The small BET value is reasonable considering the existence of solid Au cores. As shown in Figure S6 (Supporting Information), the Au element is about 75 wt % of the whole weight of GNR@CMS NPs. Since the solid Au core has no significant contribution to the surface area of the whole core–shell NPs, the calculated BET value of the porous SiO_2 shell can be up to 302 m^2/g.

It should be noted that the thickness of silica shells of GNR@CMS NPs can be altered by adjusting experimental parameters, including reaction time and the ratio of silica precursors to the GNRs. As shown in Figure S7 (Supporting Information), the thicknesses of silica shells are gradually tuned from ~9 to ~45 nm. These results indicate the flexible control over the thickness of the CMS shells by this method.

Plasmon-Induced Optical Activity of GNR@CMS NPs. Impressively, except for the existing CD absorption at ca. 230 nm originating from the chiral surfactants inside the silica shells (Figure S8a, Supporting Information), GNR@CMS NPs prepared by oppositely chiral templates (C_{16}-L-Phe or C_{16}-D-Phe) exhibit novel and strong plasmon-induced CD signals in the visible and near-IR region (black and red curves in Figure 3a). Moreover, these CD spectra show a good mirror image. In comparison, no CD signals are detected for the NPs synthesized by the racemic chiral surfactant (blue curve in Figure 3a). The intensity of plasmon-induced CD signals is believed to be determined by the coupling strength between the nonchiral metal NPs and the chiral molecules, which can be largely affected by the surface plasmon resonance features of metal NPs.[38−40] As for our experiments, the considerably small CD signals around 520 nm correspond to the weaker transverse LSPR (ca. 520 nm) of GNRs, while the large bisignate CD signals ranging from 500 nm to more than 900 nm are ascribed to the stronger longitudinal LSPR (Figure 3b). It is noticed that similar plasmon-induced optical features, a weak single CD signal at transverse LSPR position followed by strong bisignate CD signals at longitudinal LSPR positions, have been reported on the composite of GNRs and chiral anthraquinone-based oxalamde fibers.[41] Nevertheless, previous methods to obtain distinct plasmon-induced CD signals are mostly based on the adsorption of noble-metal NPs/NRs onto the chiral scaffolds[42−48] or the formation of noble-metal NP/NR aggregates.[49,50] In contrast, in our work, the GNR@CMS NPs with strong plasmon-induced CD signals are stable in solution, which provides more opportunities for solution-based applications.

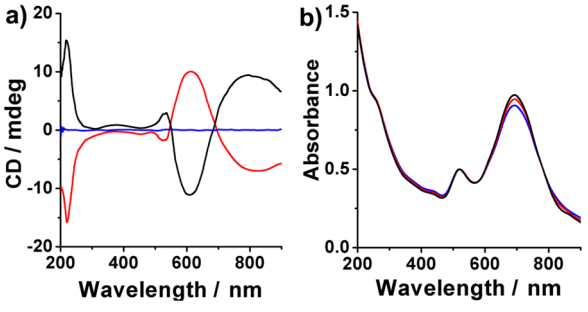

Figure 3. (a) CD and (b) UV–vis spectra of the GNR@CMS NPs templated by three types of different chiral surfactants: C_{16}-L-Phe (black); C_{16}-D-Phe (red); C_{16}-DL-Phe (blue).

Control experiments reveal the critical influence of near-field plasmons on the CD signals appearing in the visible and near-IR region. When the GNRs are simply mixed with chiral molecules in aqueous solution, no obvious CD signals in the visible range are observed, although a similar CD signal corresponding to the pure chiral molecules appears in the UV region (Figure S8b, Supporting Information). Unlike the case in the mesoporous silica shells, a simple mixture results in the preferential solubility of chiral surfactants in the solution rather than attaching on the surface of the GNRs. These results confirm that the plasmon-induced optical chiral property of GNR@CMS NPs originates from the strong near-field coupling between GNRs and chiral molecules in the mesoporous silica shells. When the chiral molecules are extracted, there is also no CD activity in the whole visible and near-IR region (Figure S9, Supporting Information), which confirms the coupling effect between the chiral molecules and the GNRs.

To realize the intended manipulation of CD activity in the visible and near-IR region is still a challenging topic.[51−53] In this work, the plasmon-induced CD signals of the GNR@CMS NPs are easily tuned in the visible and near-IR region by altering the aspect ratios of GNR cores. Figure 4 shows the CD and corresponding UV–vis spectra of a series of the GNR@CMS NPs. Two prominent optical features are observed. First, with an increase in the aspect ratios of GNR cores, the absorption peaks at around 700 nm related to longitudinal LSPR of GNRs are red-shifted (Figure 4c,d). Accordingly, plasmon-induced CD signals of both GNR@CMS NPs synthesized by L or D chiral surfactants also show gradual bathochromic shifts. Second, the CD intensities of both GNR@CMS NPs dramatically decrease with the red shift of the longitudinal LSPR (Figure 4a,b). Changes in the peak position and amplitude are both directly related to optical coupling between the chiral molecules and GNRs, which are located in the shells and cores, respectively. When the longitudinal LSPR moves to a shorter wavelength, the plasmon frequency of GNRs is much closer to the band wavelength of chiral molecules (200–300 nm, Figure S8a), leading to a stronger coupling effect. Therefore, a stronger CD signal can be achieved, as seen in Figure 4a,b. It is also evident that in comparison with the small variation in the UV–vis spectra (Figure 4c,d), the intensities of the corresponding CD spectra experience larger alternations (Figure 4a,b). These phenomena indicate that the plasmon-induced CD activity is more sensitive than the absorption amplitude of LSPR, which allows the core–

dx.doi.org/10.1021/ja312327m | J. Am. Chem. Soc. 2013, 135, 9659–9664

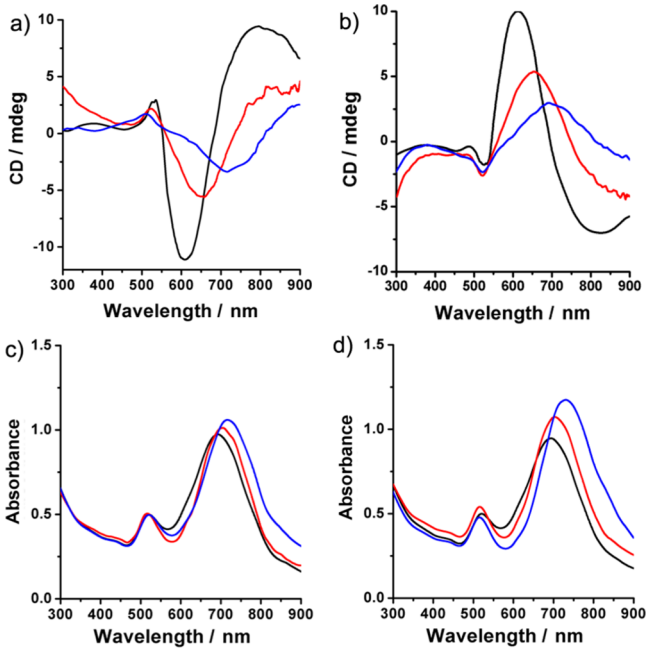

Figure 4. CD and UV−vis spectra of the GNR@CMS NPs with different aspect ratio of GNRs: (a) CD and (c) UV−vis spectra of three GNR@CMS NPs templated by C_{16}-L-Phe; (b) CD and (d) UV−vis spectra of three GNR@CMS NPs templated by C_{16}-D-Phe.

shell structures to become ideal candidates for highly sensitive biosensors and chiral detectors.

SERS of GNR@CMS NPs for Chiral Recognition. Highly sensitive chiral recognition is realized by studying the SERS response of the GNR@CMS NPs toward the chiral molecules. As the chiral Cys molecules are loaded in the porous shells, additional SERS bands are discerned in the region of 600−900 cm^{-1} in comparison with those of the freshly synthesized GNR@CMS NPs (Figure 5 and Figure S10 (Supporting Information)), and the assignment of all the SERS peaks is summarized in Table S1 (Supporting Information). Very interestingly, when the Cys and shell-template molecules are

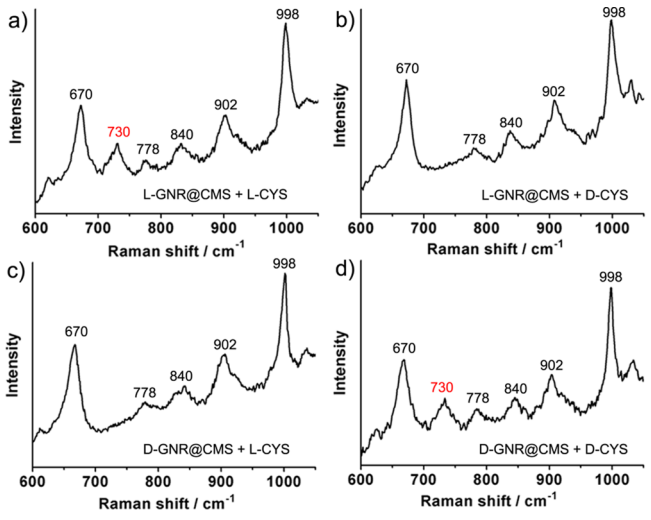

Figure 5. SERS spectra of L- and D-Cys loaded into GNR@CMS NPs with different chiral templates, as indicated in the spectra. L-GNR@CMS and D-GNR@CMS represent the core−shell structures templated by C_{16}-L-Phe and C_{16}-D-Phe, respectively.

of the same configuration (L-Cys vs C_{16}-L-Phe or D-Cys vs C_{16}-D-Phe), a new SERS peak appears at 730 cm^{-1} (Figure 5a,d); however, the 730 cm^{-1} peak is absent if the Cys and shell-template molecules have opposite chirality (Figure 5b,c). The difference in the SERS spectra is caused by the conformation change of chiral Cys molecules when they are docked inside the chiral CMS shells. Under the conditions of absence of a chiral environment, the Cys molecules prefer adopting a P_H conformation and are adsorbed on the Au surface via three functional groups, including a sulfur atom, NH_3^+ and COO^- groups (Figure 6a), and the band at 670 cm^{-1} is assigned to the

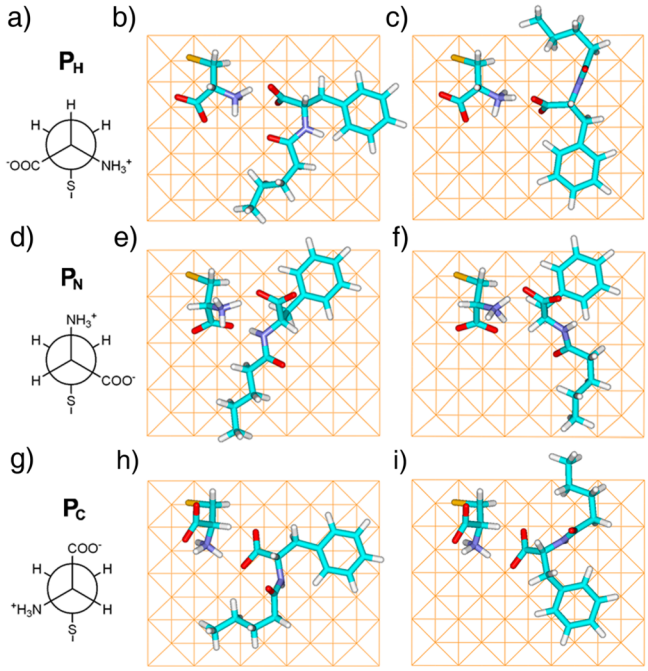

Figure 6. Scheme of P_H, P_N, and P_C conformations of L-Cys molecules on the Au surface and a simplified DFT model for the interaction manner of L-Cys on the Au surface interacting with different shell-template molecules: P_H conformation of L-Cys (a) interacting with C_{16}-L-Phe (b) and C_{16}-D-Phe (c), respectively; P_N conformation of L-Cys (d) interacting with C_{16}-L-Phe (e) and C_{16}-D-Phe (f), respectively; P_C conformation of L-Cys (g) interacting with C_{16}-L-Phe (h) and C_{16}-D-Phe (i), respectively. Color scheme: C, cyan; N, violet; O, red; S, yellow; H, white. The grid substrate represents the Au surface.

C−S stretching vibration of the P_H conformation.[54,55] As the L(or D-)-Cys molecules interact with C_{16}-L(or D-)-Phe surfactants in the CMS shells, they are forced to change from a P_H into a P_N conformation (only the S atom and COO^- group interact with the Au surface whereas the NH_3^+ group is away from the Au surface; Figure 6d), owing to the strong interaction with the chiral surfactants in the CMS shells. Thus, a new band at 730 cm^{-1} corresponding to the C−S vibration of the P_N conformation is observed.[55,56] However, when chiral Cys molecules are adsorbed into the nonchiral C_{16}-DL-Phe templated GNR@CMS NPs, the recognition effect is absent (Figure S11, Supporting Information), indicating that the SERS chiroptical property is correlated with the chiral template molecules in the shells. One can also notice that the chirality of CMS shells is maintained during the chrial recognition process, because no evident change in the plasmon-induced CD spectra of GNR@CMS NPs is distinguished before and after addition of chiral Cys molecules (Figure S12, Supporting Information).

dx.doi.org/10.1021/ja312327m | J. Am. Chem. Soc. 2013, 135, 9659−9664

To further elucidate the preferential conformations of L- and D-Cys molecules interacting with the GNR@CMS NPs, theoretical calculations were conducted by DFT methods. L-Cys molecules of P_H, P_N, and P_C conformations were chosen, and their interactions with both GNR surfaces and the shell-template molecules were systematically evaluated (see details in the theoretical calculation part in the Supporting Information). Because the long alkane chain in C_{16}-L-Phe or C_{16}-D-Phe has no interaction with Cys molecules, the DFT model was simplified by decreasing the alkane chain to 4 carbons rather than 15. The simplified DFT models are illustrated in Figure 6, and the corresponding calculation results are summarized in Table 1.

Table 1. Interaction Energies of Different Conformations of L-Cys Molecules with both the GNR Substrates and the Shell-Template Molecules[a]

conformation	C_{16}-L-Phe (kcal/mol)	C_{16}-D-Phe (kcal/mol)
P_H	−244.21	−244.27
P_N	−243.66	−239.24
P_C	−223.27	−218.82

[a]Here, the more negative energy means the system is more stable.

Evidently, if L-Cys interacts with C_{16}-L-Phe on the GNR surface (the second column in Table 1), the interaction energy difference between P_H and P_N conformations is only 0.55 kcal/mol, whereas the interaction energy of P_C is much higher. This is why in the SERS spectrum (Figure 5a) one can see both 670 and 730 cm^{-1} bands corresponding to P_H and P_N conformations, respectively. In comparison, when L-Cys interacts with C_{16}-D-Phe on the GNR surface (the third column in Table 1), the interaction energy of the P_H conformation is 5.03 kcal/mol lower than that of the P_N conformation. This energy difference is considerably larger than that of thermal energy at room temperature (0.59 kcal/mol). Therefore, the conformation change from P_H to P_N types is energetically unfavorable and the SERS peak at 730 cm^{-1} is absent (Figure 5b). In addition, the P_C conformation is the most unstable conformation, with the highest interaction energy in either of the two shell-template molecules, and should not exist in the shell. It is clear that the theoretical calculations (Table 1) are in good agreement with our experimental results (Figure 5).

Finally, the quantitative determination of the amount of Cys enantiomers in solution was carried out. When the solution containing Cys enantiomers was mixed with the C_{16}-L-Phe templated GNR@CMS NPs, the peak intensity at 730 cm^{-1} in SERS spectra decreased with a decrease in the ratio of L-Cys in the mixture of enantiomers (Figure 7a). A similar phenomenon was also explored for the case of the GNR@CMS NPs templated by C_{16}-D-Phe (Figure S13, Supporting Information). The reason is that because the SERS peak at 730 cm^{-1} appears only when Cys and shell-template molecules are of the same chirality, more L-Cys molecules give rise to a higher SERS peak intensity. The peak intensity at 730 cm^{-1} is further plotted as a function of the percentage of L-Cys (Figure 7b), which presents a good linear relationship with a correlation coefficient of 0.9612. In addition, the detection limit for the chiral Cys is as low as 50 μM (Figure S14, Supporting Information), permitting the low-concentration detection of chiral molecules. Altogether, the GNR@CMS NPs provide a promising platform for semiquantitative and sensitive determinations of the ratio of enantiomers in the mixtures on the basis of their SERS responses.

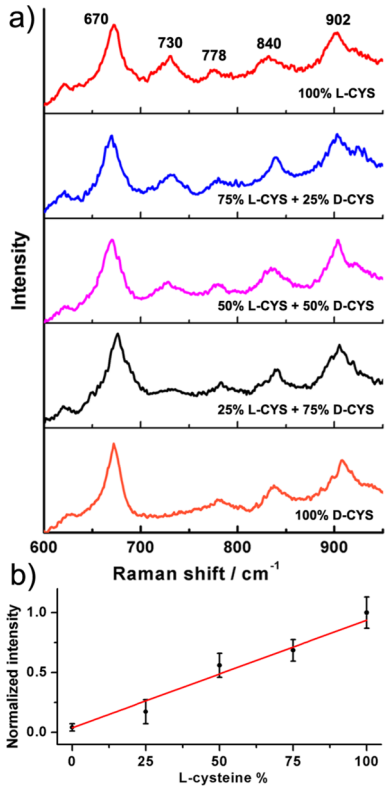

Figure 7. (a) SERS for the solution containing Cys of different enantiomer ratios mixed with GNR@CMS NPs templated by C_{16}-L-Phe. (b) Relative SERS peak intensity at 730 cm^{-1} plotted as a function of the percentage of L-Cys in the enantiomer mixture and the corresponding linear-fitting result (red line, R^2 = 0.9612).

CONCLUSION

In conclusion, GNR@CMS NPs with unique optical performance, including CD activity and SERS response, have been successfully prepared for the first time. These novel core−shell NPs exhibit distinctive plasmon-induced CD signals in the visible range through strong optical coupling between GNRs and chiral molecules in the mesopores of silica shells. It is noteworthy that the CD activity of the core−shell NPs can be manipulated in a large range by altering the aspect ratio of the GNRs. More importantly, the GNR@CMS NPs demonstrate high chiral recognition ability of Cys molecules on the basis of SERS detection, which highlights their potential applications. Since this synthesis approach can be easily extended to various types of inorganic NPs such as magnetic NPs, quantum dots, and metal oxide NPs, it is highly expected that these types of composite NPs, which combine the excellent optical/electrical/magnetic/catalytic properties registered in inorganic cores and the specific recognition function arising from chiral shells, will open up many application opportunities in the fields of chiral recognition or separation, asymmetric catalysis, and biosensors.

ASSOCIATED CONTENT

Supporting Information

Text giving theoretical calculation details, tables giving additional data, and additional figures. This material is available free of charge via the Internet at http://pubs.acs.org.

dx.doi.org/10.1021/ja312327m | J. Am. Chem. Soc. 2013, 135, 9659−9664

AUTHOR INFORMATION

Corresponding Author

*E-mail: zytang@nanoctr.cn (Z.T.); chesa@sjtu.edu.cn (S.C.); gaoyan@nanoctr.cn (Y.G.).

Author Contributions

§These authors contributed equally.

Notes

The authors declare no competing financial interest.

ACKNOWLEDGMENTS

This work was supported financially by the National Natural Science Foundation for Distinguished Youth Scholars of China (21025310, Z.T.), the National Natural Science Foundation of China (21003026, 20933008 and 51272047, Y.G.; 20973047 and 91027011, Z.T.), and the National Research Fund for Fundamental Key Project (2009CB930401, Z.T.; 2012CB933001, K.D.).

REFERENCES

(1) Daniel, M. C.; Astruc, D. *Chem. Rev.* **2004**, *104*, 293.
(2) Noguez, C.; Garzón, I. L. *Chem. Soc. Rev.* **2009**, *38*, 757.
(3) Sudeep, P. K.; Joseph, S. T. S.; Thomas, K. G. *J. Am. Chem. Soc.* **2005**, *127*, 6516.
(4) Burda, C.; Chen, X. B.; Narayanan, R.; El-Sayed, M. A. *Chem. Rev.* **2005**, *105*, 1025.
(5) Tong, L.; Zhao, Y.; Huff, T. B.; Hansen, M. N.; Wei, A.; Cheng, J. X. *Adv. Mater.* **2007**, *19*, 3136.
(6) Nikoobakht, B.; El-Sayed, M. A. *Chem. Mater.* **2003**, *15*, 1957.
(7) Pérez-Juste, J.; Pastoriza-Santos, I.; Liz-Marzán, L. M.; Mulvaney, P. *Coord. Chem. Rev.* **2005**, *249*, 1870.
(8) Jana, N. R.; Gearheart, L.; Murphy, C. J. *J. Phys. Chem. B* **2001**, *105*, 4065.
(9) Smith, D. K.; Korgel, B. A. *Langmuir* **2008**, *24*, 644.
(10) Smith, D. K.; Miller, N. R.; Korgel, B. A. *Langmuir* **2009**, *25*, 9518.
(11) Cozzoli, P. D.; Pellegrino, T.; Manna, L. *Chem. Soc. Rev.* **2006**, *35*, 1195.
(12) Zhang, L.; Qiao, S. Z.; Jin, Y. G.; Chen, Z. G.; Gu, H. C.; Lu, G. Q. *Adv. Mater.* **2008**, *20*, 805.
(13) Liu, J.; Qiao, S. Z.; Hartono, S. B.; Lu, G. Q. *Angew. Chem., Int. Ed.* **2010**, *49*, 4981.
(14) Guerrero-Martínez, A.; Pérez-Juste, J.; Liz-Marzán, L. M. *Adv. Mater.* **2010**, *22*, 1182.
(15) Liz-Marzán, L. M.; Giersig, M.; Mulvaney, P. *Langmuir* **1996**, *12*, 4329.
(16) Pastoriza-Santos, I.; Pérez-Juste, J.; Liz-Marzán, L. M. *Chem. Mater.* **2006**, *18*, 2465.
(17) Heitsch, A. T.; Smith, D. K.; Patel, R. N.; Ress, D.; Korgel, B. A. *J. Solid State Chem.* **2008**, *181*, 1590.
(18) Corma, A.; Garcia, H. *Chem. Soc. Rev.* **2008**, *37*, 2096.
(19) Liu, R.; Liao, P. H.; Liu, J. K.; Feng, P. Y. *Langmuir* **2011**, *27*, 3095.
(20) Zhang, H.; Sun, J. M.; Ma, D.; Bao, X. H.; Klein-Hoffmann, A.; Weinberg, G.; Su, D. S.; Schlögl, R. *J. Am. Chem. Soc.* **2004**, *126*, 7440.
(21) Zuloaga, J.; Prodan, E.; Nordlander, P. *ACS Nano* **2010**, *4*, 5269.
(22) Lee, A.; Andrade, G. F. S.; Ahmed, A.; Souza, M. L.; Coombs, N.; Tumarkin, E.; Liu, K.; Gordon, R.; Brolo, A. G.; Kumacheva, E. *J. Am. Chem. Soc.* **2011**, *133*, 7563.
(23) Osberg, K. D.; Rycenga, M.; Harris, N.; Schmucker, A. L.; Langille, M. R.; Schatz, G. C.; Mirkin, C. A. *Nano Lett.* **2012**, *12*, 3828.
(24) Xu, L. G.; Kuang, H.; Xu, C. L.; Ma, W.; Wang, L. B.; Kotov, N. A. *J. Am. Chem. Soc.* **2012**, *134*, 1699.
(25) Zijlstra, P.; Paulo, P. M. R.; Orrit, M. *Nat. Nanotechnol.* **2012**, *7*, 379.
(26) Che, S.; Liu, Z.; Ohsuna, T.; Sakamoto, K.; Terasaki, O.; Tatsumi, T. *Nature* **2004**, *429*, 281.
(27) Qiu, H. B.; Inoue, Y.; Che, S. *Angew. Chem., Int. Ed.* **2009**, *48*, 3069.
(28) Yokoi, T.; Ogawa, K.; Lu, D. L.; Kondo, J. N.; Kubota, Y.; Tatsumi, T. *Chem. Mater.* **2011**, *23*, 2014.
(29) Meng, X. J.; Yokoi, T.; Lu, D. L.; Tatsumi, T. *Angew. Chem., Int. Ed.* **2007**, *46*, 7796.
(30) Jung, J. H.; Kobayashi, H.; Masuda, M.; Shimizu, T.; Shinkai, S. *J. Am. Chem. Soc.* **2001**, *123*, 8785.
(31) Sato, I.; Kadowaki, K.; Urabe, H.; Jung, J. H.; Ono, Y.; Shinkai, S.; Soai, K. *Tetrahedron Lett.* **2003**, *44*, 721.
(32) Baev, A.; Samoc, M.; Prasad, P. N.; Krykunov, M.; Autschbach, J. *Opt. Express.* **2007**, *15*, 5730.
(33) Su, D. S. *Angew. Chem., Int. Ed.* **2011**, *50*, 4747.
(34) Chen, Y. T.; Wang, H. P.; Liu, C. J.; Zeng, Z. Y.; Zhang, H.; Zhou, C. M.; Jia, X. L.; Yang, Y. H. *J. Catal.* **2012**, *289*, 105−117.
(35) Guo, Z.; Du, Y.; Liu, X. B.; Ng, S. C.; Chen, Y.; Yang, Y. H. *Nanotechnology* **2010**, *21*, 165103.
(36) Guo, Z.; Du, Y.; Chen, Y. T.; Ng, S. C.; Yang, Y. H. *J. Phys. Chem. C* **2010**, *114*, 14353−14361.
(37) Takehara, M.; Takizawa, K.; Yoshimur., I.; Yoshida, R. *J. Am. Oil Chem. Soc.* **1972**, *49*, 157.
(38) Govorov, A. O. *J. Phys. Chem. C* **2011**, *115*, 7914.
(39) Govorov, A. O.; Fan, Z. Y.; Hernandez, P.; Slocik, J. M.; Naik, R. R. *Nano Lett.* **2010**, *10*, 1374.
(40) Auguié, B.; Alonso-Gómez, J. L.; Guerrero-Martínez, A.; Liz-Marzán, L. M. *J. Phys. Chem. Lett.* **2011**, *2*, 846.
(41) Guerrero-Martínez, A.; Auguié, B.; Alonso-Gómez, J. L.; Džolić, Z.; Gómez-Graña, S.; Žinić, M.; Cid, M. M.; Liz-Marzán, L. M. *Angew. Chem., Int. Ed.* **2011**, *50*, 5499.
(42) Gautier, C.; Bürgi, T. *J. Am. Chem. Soc.* **2006**, *128*, 11079.
(43) Shemer, G.; Krichevski, O.; Markovich, G.; Molotsky, T.; Lubitz, I.; Kotlyar, A. B. *J. Am. Chem. Soc.* **2006**, *128*, 11006.
(44) Chen, W.; Bian, A.; Agarwal, A.; Liu, L. Q.; Shen, H. B.; Wang, L. B.; Xu, C. L.; Kotov, N. A. *Nano Lett.* **2009**, *9*, 2153.
(45) Qi, H.; Shopsowitz, K. E.; Hamad, W. Y.; MacLachlan, M. J. *J. Am. Chem. Soc.* **2011**, *133*, 3728.
(46) George, J.; Thomas, K. G. *J. Am. Chem. Soc.* **2010**, *132*, 2502.
(47) Slocik, J. M.; Govorov, A. O.; Naik, R. R. *Nano Lett.* **2011**, *11*, 701.
(48) Zhou, Y. L.; Yang, M.; Sun, K.; Tang, Z. Y.; Kotov, N. A. *J. Am. Chem. Soc.* **2010**, *132*, 6006.
(49) Zhu, Z. N.; Liu, W. J.; Li, Z. T.; Han, B.; Zhou, Y. L.; Gao, Y.; Tang, Z. Y. *ACS Nano* **2012**, *6*, 2326.
(50) Li, Z. T.; Zhu, Z. N.; Liu, W. J.; Zhou, Y. L.; Han, B.; Gao, Y.; Tang, Z. Y. *J. Am. Chem. Soc.* **2012**, *134*, 3322.
(51) Lacasta, S.; Sebastián, V.; Casado, C.; Mayoral, A.; Romero, P.; Larrea, A.; Vispe, E.; López-Ram-de-Viu, P.; Uriel, S.; Coronas, J. *Chem. Mater.* **2011**, *23*, 1280.
(52) Fireman-Shoresh, S.; Marx, S.; Avnir, D. *J. Mater. Chem.* **2007**, *17*, 536.
(53) Zhao, J. S.; Ruan, Y. B.; Zhou, R.; Jiang, Y. B. *Chem. Sci.* **2011**, *2*, 937.
(54) Jing, C. Y.; Fang, Y. *Chem. Phys.* **2007**, *332*, 27.
(55) Graff, M.; Bukowska, J. *Vib. Spectrosc.* **2010**, *52*, 103.
(56) Graff, M.; Bukowska, J. *J. Phys. Chem. B* **2005**, *109*, 9567.